1-1-2007

A Simplified Model Of Heat And Mass Transfer Between Air And Falling-Film Desiccant In A Parallel-Plate Dehumidifier

Anna Kathrine Hueffed

A SIMPLIFIED MODEL OF HEAT AND MASS TRANSFER BETWEEN AIR AND FALLING-FLM DESICCANT IN A PARALLEL-PLATE DEHUMIDIFIER

By

Anna Kathrine Hueffed

A Thesis
Submitted to the Faculty of
Mississippi State University
in Partial Fulfillment of the Requirements
for the Degree of Master of Science
in Mechanical Engineering
in the Department of Mechanical Engineering

Mississippi State, Mississippi

December 2007

A SIMPLIFIED MODEL OF HEAT AND MASS TRANSFER BETWEEN AIR AND FALLING-FILM DESICCANT IN A PARALLEL-PLATE DEHUMIDIFIER

By

Anna Kathrine Hueffed

Approved:

Louay M. Chamra Professor of Mechanical Engineering Acting Department Head of Mechanical Engineering (Director of Thesis)	Pedro Mago Assistant Professor of Mechanical Engineering (Committee Member)
B.K. Hodge Professor of Mechanical Engineering (Committee Member)	Steve Daniewicz Professor of Mechanical Engineering (Graduate Coordinator)

W. Glenn Steele
Interim Dean of the Bagley College of Engineering

Name: Anna Kathrine Hueffed

Date of Degree: December 14, 2007

Institution: Mississippi State University

Major Field: Mechanical Engineering

Major Professor: Dr. Louay M. Chamra

Title of Study: A SIMPLIFIED MODEL OF HEAT AND MASS TRANSFER BETWEEN AIR AND FALLING-FILM DESICCANT IN A PARALLEL-PLATE DEHUMIDIFIER

Pages in Study: 54

Candidate for Degree of Master of Science

A simplified model is developed to predict the heat and mass transfer between air and falling-film liquid desiccant during dehumidification in a parallel-plate absorber. Compared to second-order partial differential equations that describe fluid motion, first-order, non-coupled, ordinary differential equations are used to estimate the heat and mass transferred and explicit equations are derived from conservation principles to yield the exiting absorber conditions for different flow arrangements. The model uses a control volume approach that accounts for the change in film thickness and property values. The model results were within 5% of a more complicated parallel-flow model in literature. Using existing experimental data for a counterflow absorber, the model uncertainty was determined and the model was validated at the level of 8.5 % for varying inlet desiccant mass flow rates and 11% for varying inlet air mass flow rates.

ACKNOWLEDGEMENTS

The author expresses her sincere gratitude for all the invaluable assistance and advice that was received during this research. I would like to thank my advisor Dr. Louay Chamra for his guidance and support while completing my degree requirements. I would also like to thank Dr. Pedro Mago, Nelson Fumo, and Dr. B. Keith Hodge for their help and cooperation during the preparation of this thesis.

TABLE OF CONTENTS

APPENDIX

LIST OF TABLES

LIST OF FIGURES

NOMENCLATURE

A_c	cross-sectional area (m^2)
C_a	concentration of water in air mixture (kg_w/kg_a)
C_d	concentration of desiccant in solution (kg_d/kg_s)
C_I	equilibrium water concentration of air at desiccant-air interface (kg_w/kg_a)
CV	control volume
c_p	specific heat (J/kg-K)
D	mass diffusivity (m^2/s)
D_h	hydraulic diameter (m)
d	experimental data
g	acceleration due to gravity (m/s^2)
h	enthalpy (kJ/kg)
$h_{g.0^\circ C}$	enthalpy of saturated water vapor at 0°C (kJ/kg)
h_h	heat transfer coefficient (W/m^2-K)
h_m	mass transfer coefficient (m/s)
k	thermal conductivity (W/m-K)
m	model result
$\dot{m}_a$	mass flow rate of air per channel (kg/s)

$\dot{m}_d$	mass flow rate of desiccant per plate (kg/s)
$\dot{m}_w$	mass flow rate of water (kg/s)
MW	molecular weight
Nu	Nusselt number
Nx	number of control volumes in x-direction
Ny	number of control volumes in y-direction
P	pressure (Pa)
$P_{v.d}$	surface vapor pressure of desiccant solution (Pa)
P_w	saturation pressure of water vapor (Pa)
P_{wetted}	wetted perimeter (m)
Q_c	convective heat transfer (W)
T	temperature (°C)
U_E	uncertainty of comparison error, validation uncertainty
U_d	uncertainty of experimental data
U_m	uncertainty of model result
U_{Y_j}	uncertainty of input parameter
UMF	uncertainty magnification factor
UPC	uncertainty percent contribution (%)
W_a	humidity ratio of air (kg_w/kg_{da})
w	plate spacing (m)
X	plate width (m)
x	coordinate normal to film and tangent to plate

Y	plate height (m)
Y_j	input parameter
y	coordinate parallel to desiccant flow
z	coordinate normal to plate

Greek

α	thermal diffusivity (m^2/s)
β	mass transfer coefficient calculated by Kessling et al. (1998) (m/s)
δ_d	desiccant film thickness (m)
ζ_d	concentration of water in desiccant solution (kg_w/kg_s)
ρ	density (kg/m^3)
μ	dynamic viscosity ($N\text{-}s/m^2$)

Subscripts

a	air mixture of dry air and water vapor
d	desiccant
da	dry air
f	saturated liquid water
g	saturated water vapor
m	control volume index
n	control volume index
s	desiccant solution
w	water
wv	water vapor

i	inlet
e	exit

CHAPTER 1

INTRODUCTION AND LITERATURE REVIEW

1.1 Introduction

Within the past few years the cost of electricity, grid stability, and global warming have become growing concerns which are leading to alternative sources of energy generation and a primary focus on the efficient use of energy. One such area of interest is energy use in buildings where heating, ventilating, air conditioning, humidity control, and indoor air quality are important factors that also consume a large portion of the energy supplied to the building. Desiccant technologies can provide improved humidity control and increased efficiency in place of or when coupled with traditional air conditioning methods, typically vapor compression cycles.

Desiccants, either solid or liquid, are materials that attract and hold water vapor. During dehumidification water is directly transferred from the air and either adsorbed or absorbed into the desiccant solution because of a difference in vapor pressure between the water vapor in the air and the equilibrium vapor pressure of water in the air at the air-desiccant interface. This equilibrium vapor pressure is more easily referred to as the vapor pressure of the desiccant. The reverse process of removing water from the desiccant solution to allow it to be reused is called regeneration and is driven by heat. In contrast, the vapor compression cycle uses an electric compressor to cool the air below its

dew point to condense water out of the air stream. The air must then be reheated to the desired temperature.

Solid desiccant systems are more established than liquid desiccant systems and have found success in heating, ventilating, and air conditioning applications. Currently, liquid desiccant systems are primarily limited to uses in industrial applications where exhaust heat is readily available or in applications where strict humidity control is required such as supermarkets, ice rinks, or food processing plants. These limitations can partially be attributed to the corrosive nature of some liquid desiccants and the possibility of desiccant to be entrained in the process air.

The potential for liquid desiccant systems exists due to their advantages over solid desiccants. Solid desiccants have to be regenerated at temperatures between 80°C and 100°C, but liquid desiccants can be regenerated at lower temperatures, between 50°C and 80°C, which allows regeneration from heat sources such as solar energy. Lower air-side pressure losses reduce the required parasitic power, which is especially important for high ventilation rates. In addition, liquid desiccants have the ability to filter the air of potentially hazardous air born bacteria allowing for better indoor air quality and reduced risk of "sick-building" syndrome. Unlike solid desiccant systems where the desiccant is permanently affixed to the rotor of a rotary heat exchanger, liquid desiccant systems can take advantage of internal cooling to reduce the desiccant solution temperature. Internal cooling can provide both sensible and latent cooling, effectively eliminating the need for addition cooling methods. Finally, liquid desiccant systems have a lower initial cost and operating cost than solid desiccant counterparts.

The most common types of liquid desiccants employed are halide salts such as lithium chloride (LiCl), lithium bromide (LiBr), and calcium chloride ($CaCl_2$) in solution with water. One disadvantage of halide salts is their corrosive nature which can pose problems for ferrous components. Another common liquid desiccant is tryethyl glycol which is commonly used in the food processing industry because it is not corrosive. However, large amounts of glycol evaporate during regeneration due to its high vapor pressure at regeneration temperatures.

Liquid desiccant systems consist of two main components, the absorber, or conditioner, where dehumidification occurs and the regenerator where the dilute desiccant solution is regenerated to a concentrated solution. Prior to entering the absorber, the concentrated desiccant is cooled to lower its vapor pressure. The vapor pressure of the solution increases with an increase in temperature and with increased moisture content, as illustrated in Figure 1.1. The solution vapor pressure is lower than the vapor pressure of the incoming air, so water is transferred from the air to the desiccant solution which dilutes the desiccant concentration and usually increases its temperature. Upon exiting the absorber, the dilute desiccant is further heated to raise its vapor pressure before entering the regenerator where the solution is exposed to a regenerative air stream. The air stream has a lower vapor pressure than the desiccant solution allowing water to exit the desiccant solution. The energy used to heat the desiccant solution can be supplied by a gas burner, waste exhaust heat from an industrial process or cooling, heating, and power (CHP) applications, solar applications, or waste heat from the compressor of either a vapor compression cycle or an absorption cycle.

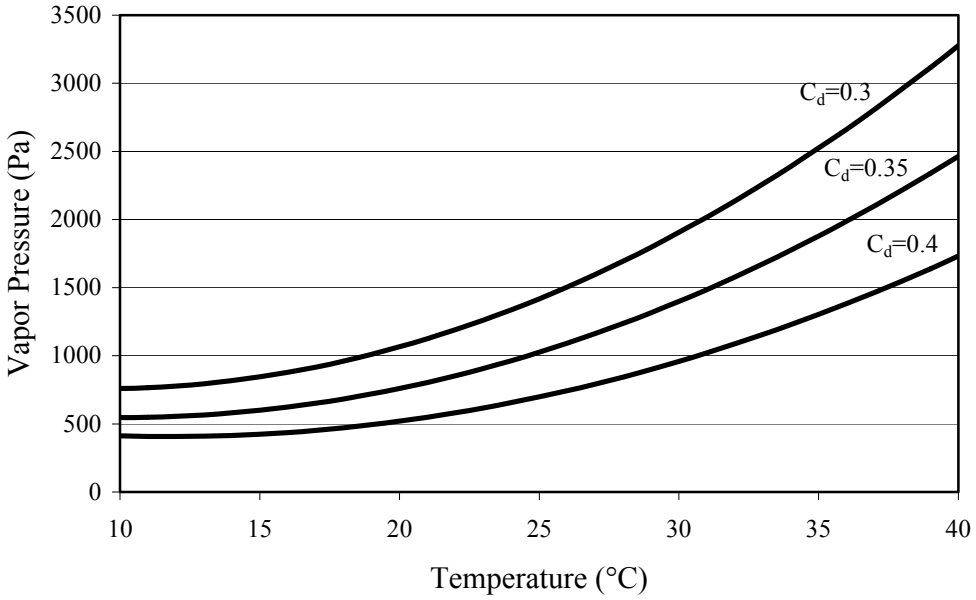

Figure 1.1 Vapor pressure of LiCl as a function of desiccant temperature and concentration

The absorption process can be classified as adiabatic or isothermal. Adiabatic absorption occurs in the absence of internal cooling. During this process the temperature of the air and the desiccant will increase due to the latent heat of the absorbed water vapor. The air can then be cooled to the desired temperature using cooling coils of a vapor compression cycle or an evaporative cooler. This allows the latent and sensible loads to be handled independently yielding better humidity control and a decrease in the load of the vapor compression cycle allowing downsized equipment and lower electric demand. Isothermal absorption results from internal cooling which effectively removes the heat of absorption and has the potential to provide simultaneous dehumidification and cooling of the air.

Most absorbers and regenerators in liquid desiccant systems are either a packed-bed tower or a parallel-plate heat exchanger. Packed-bed towers, presented in Figure 1.2, spray desiccant down onto packed beds with the air flowing through the packing. The packing allows a large surface area of the desiccant to be exposed to the air stream over a long contact time. These systems are usually compact, but require a high solution flow rate for efficient dehumidification to account for the absorbed latent heat. In addition, packed beds results in large pressure losses and have the potential risk of solution carry over, where desiccant solution is entrained in the process air flow and, if not filtered out properly, can contaminate the air. Parallel-plate absorbers utilize a film of desiccant that is distributed across a vertical plate. The absorber, pictured in Figure 1.3, consists of multiple parallel-plates with the air flowing through the gaps in the plates. For a process air flow rate of 0.47 m^3/s, the solution flow rate in a parallel-plate absorber is about 32 mL/s versus conventional packed-bed conditioners that have a solution flow rate between 630 and 946 mL/s [Lowenstein et al. (2006)]. This much lower desiccant flow rate prevents the entrainment of desiccant solution in the air flow, thus eliminating the need for filters and reducing the overall maintenance of the system. Parallel-plate absorbers are often internally cooled where cool water or a refrigerant flows through the plates resulting in isothermal absorption and more efficient dehumidification over adiabatic absorption.

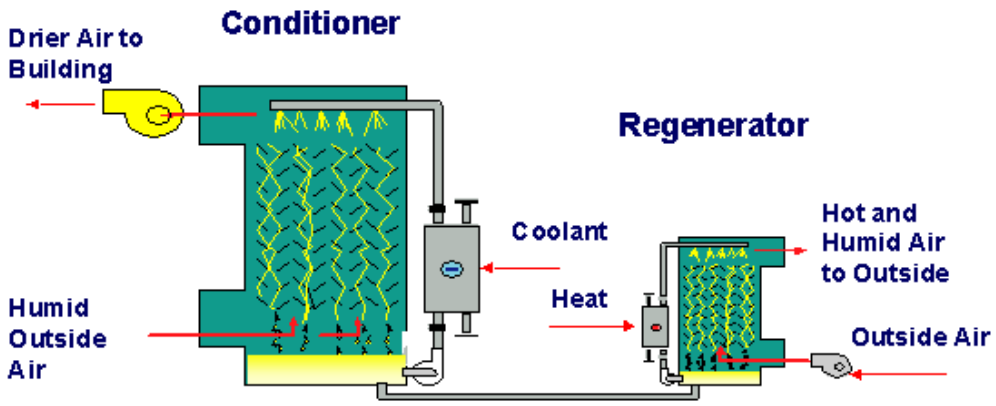

Figure 1.2 Packed-bed absorber [U.S. DOE]

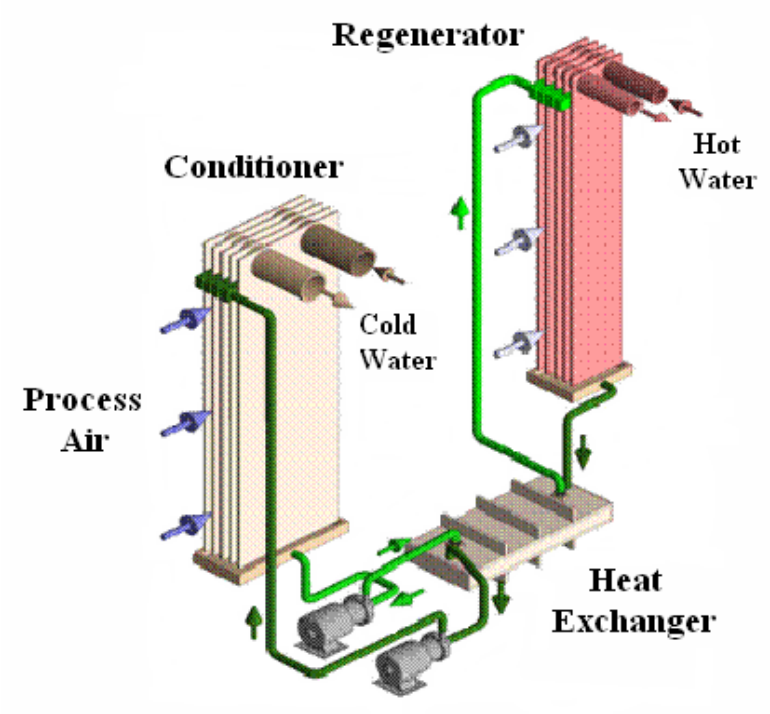

Figure 1.3 Parallel-plate conditioner [Lowenstein et al. (2006)]

The current study analyzes liquid desiccant dehumidification in a parallel-plate absorber. The heat and mass transfer process are investigated and exiting conditions are predicted using a simplified control volume model.

1.2 Literature Review

Löf (1955) first introduced the idea of liquid desiccant dehumidification using solar energy, and since then packed-beds that utilize spray towers have become the dominant construction and research area for liquid desiccant systems. Jain et al. (2007) provided a comprehensive comparative parametric analysis of packed-bed dehumidifiers along with a brief general overview of liquid desiccant technology. In comparison to packed-beds, the study and application of parallel-plate systems is limited, but increasing due to potential advantages, primarily the ability to cool the desiccant film during dehumidification.

Park et al. (1994) numerically and experimentally studied the heat and mass transfer for a crossflow configuration of air and triethylene glycol desiccant. The desiccant was distributed over the fins of a plate-fin-tube heat exchanger with refrigerant flowing through the tubes. The numerical model is more complex than parallel or counterflow arrangements because it is three-dimensional. For low air flow rates, the experiment yielded better dehumidification and the numerical predictions followed experimental trends.

Kessling et al. (1998a) investigated the use of liquid desiccant as a means of energy storage for applications where low temperature heat may not always be available. The storage capacity was defined to be the dehumidification enthalpy divided by the

volume of the diluted salt solution. To obtain a high storage capacity, a large difference between the inlet (strong) salt concentration and the exiting (weak) salt concentration is required and achieved with a low solution flow. Experiments were conducted for a setup that consisted of internally cooled parallel-plates with water flowing horizontally though the plates, desiccant flowing down the plates, and air flowing upward between the plates. Micro-porous tubes on top of each plate distributed desiccant solution flow over the width of the plate. Each plate was made of polypropylene, PP, and covered with a fleece to enable solution distribution on the hydrophobic PP-surface by capillary forces. A solution flow of about 0.21 L/m^2 could be uniformly distributed over the surface of the plates; however, after several experiments the wetted fraction was only observed to be about 30% due to poor performance of the fleece.

Kessling et al. (1998b) studied efficient dehumidification for use in energy storage. For energy storage to be possible the absorption process must be cooled and the ratio of the air to solution mass flow rate must be 50 to 100 kg/kg. Three series of experiments were performed using LiCl as the desiccant in a similar setup as Kessling et al. (1998a), although a new proprietary coating was used to solve the problem of a reliable and complete coverage of the desiccant over the plate even at low flow rates. Two absorption experiments with variable solution mass flow rates and variable air mass flow rates and a condensation experiment with different air mass flow rates were carried out. For the absorption experiments the exiting conditions were reported. The dehumidification, storage capacity, and NTU were determined and plotted versus different mass ratios. In addition, a finite difference model was used to estimate the mass transfer coefficient, β, for each experiment's inlet and exiting conditions. In the

condensation experiments, mass was transferred when the plate's surface temperature was below the dew point. This mass transfer mechanism was the same for absorption and thus provided the maximum achievable values for the mass transfer coefficient. No difference between the condensation and absorption experiments that used variable air mass flow rates could be detected. This means the plate's surface was fully covered by the solution and the distribution over the width of the plate was uniform. In addition, the condensation experiment showed that the mass transfer resistance within the solution film was negligible when compared to the resistance within the air boundary layer.

Rahamah et al. (1998) numerically investigated the heat and mass transfer process between a falling $CaCl_2$ film and air in parallel flow for isothermal absorption for a desiccant film of constant thickness. The effects of varying the inlet conditions of the air and desiccant along with the channel height were demonstrated. The investigation showed that changes in the inlet desiccant temperature had no effect since the film temperature reached the wall temperature within a very short distance of the absorber entrance, which also explains why the temperatures of the desiccant solution and air flow were not influenced by other parameters. Rahamah et al. verified that lower air flow rates give better dehumidification and cooling because of increased contact time between the air and desiccant surface and concluded that increases in the desiccant mass flow rate allowed for better dehumidification. In addition, the dehumidification process was improved by raising the inlet desiccant concentration, which is limited by crystallization of the salt in the solution. Finally, increasing the inlet humidity ratio increased the dehumidification rate. In addition to the parametric study, Rahamah et al. developed new

correlations for Nusselt and Sherwood numbers in terms or Prandtl, Reynolds, wall spacing, and channel height.

Ali et al. (2003) numerically compared parallel and counterflow configurations of air and falling film $CaCl_2$ desiccant under isothermal conditions for a desiccant film of constant thickness. In addition, copper nanoparticles were suspended in the desiccant solution in an attempt to enhance the heat and mass transfer. A parametric analysis was performed to explore the effects of the air and desiccant Reynolds numbers, channel height, and volume fraction of copper nanoparticles. The volume fraction provided little enhancement to the dehumidification and cooling process due to the small thickness of the desiccant film. When comparing the parallel-flow and counterflow arrangements the parallel-flow arrangement provided better dehumidification and cooling of the air for all parameters while the counterflow provided better regeneration rates of the desiccant at low desiccant Reynolds numbers and varying channel heights.

Ali et al. (2004) performed a similar numerical computation and parametric study for a crossflow arrangement. Low air Reynolds numbers increased the dehumidification and cooling of the air, and low solution Reynolds numbers increased dehumidification and cooling up to a point where the effect of increased solution temperature from high Reynolds numbers raised the exiting humidity and air temperature. Increasing the channel height and length increased the residual time and contact surface area between the air and desiccant thus allowing for greater reduction of the exiting humidity ratio and air temperature. Decreasing the channel spacing also yielded better dehumidification and cooling.

Mesquita et al. (2006) numerically investigated parallel and counterflow arrangements for an isothermal wall. Three models were developed. The first model used a constant desiccant film thickness by neglecting the rate of water vapor absorption into the desiccant film. The second model accounted for the water vapor absorption and used a variable desiccant film thickness and a varying desiccant mass flow rate. The final model is a simplified model that decoupled the heat and mass transfer processes to result in two independent first order differential equations for energy and species. The process was decoupled by neglecting the latent heat of absorption because it was immediately removed by the internal cooling. The heat transfer coefficient in the simplified model was determined from a Nusselt number correlation and the mass transfer coefficient was determined from the Chilton-Colburn analogy. At high desiccant flow rates, about equal to the air mass flow rate, the variable-thickness model agrees with the constant thickness model within about 1.2%. However, for low desiccant flow rates, about 400 times smaller than the air mass flow rate, differences of about 19% arose. In comparison to the experiments conducted by Kessling et al. (1998b), the temperature results agreed but the outlet humidity ratio only agreed for lower desiccant flow rates with unexplainable differences up to 13% for increased desiccant flow rates. The constant thickness and simplified models under predicted dehumidification, especially for low desiccant flow rates.

Large initial costs combined with limited research restrict experiments on parallel-plate dehumidifiers giving rise to numerical models. In general, numerical models previously discussed solve the second-order partial differential equations that

describe fluid motion for each flow stream using interfacial equilibrium conditions and prescribed boundary conditions.

This thesis develops a simplified model that uses a control volume approach in which simplified equations determine the rates of water and heat that is transferred and basic conservation principles determine the exiting conditions for a parallel-plate conditioner. The model formulation for a control volume is developed in the following section followed by the model procedure for each flow arrangement. Results are presented and compared to available data from the literature. An uncertainty analysis is performed and used in the validation of the model.

CHAPTER 2

MODEL DEVELOPMENT

2. 1 Mathematical Formulation of Elemental Control Volume

In order to predict the overall performance of a parallel-plate absorber only one channel of the absorber must be investigated, as each channel behaves independently. The schematic for one channel is presented in Figure 2.1 for (a) crossflow, (b) parallel, and (c) counterflow arrangements. In every case, the desiccant solution flows down the inner side of each plate while the air flows through the channel.

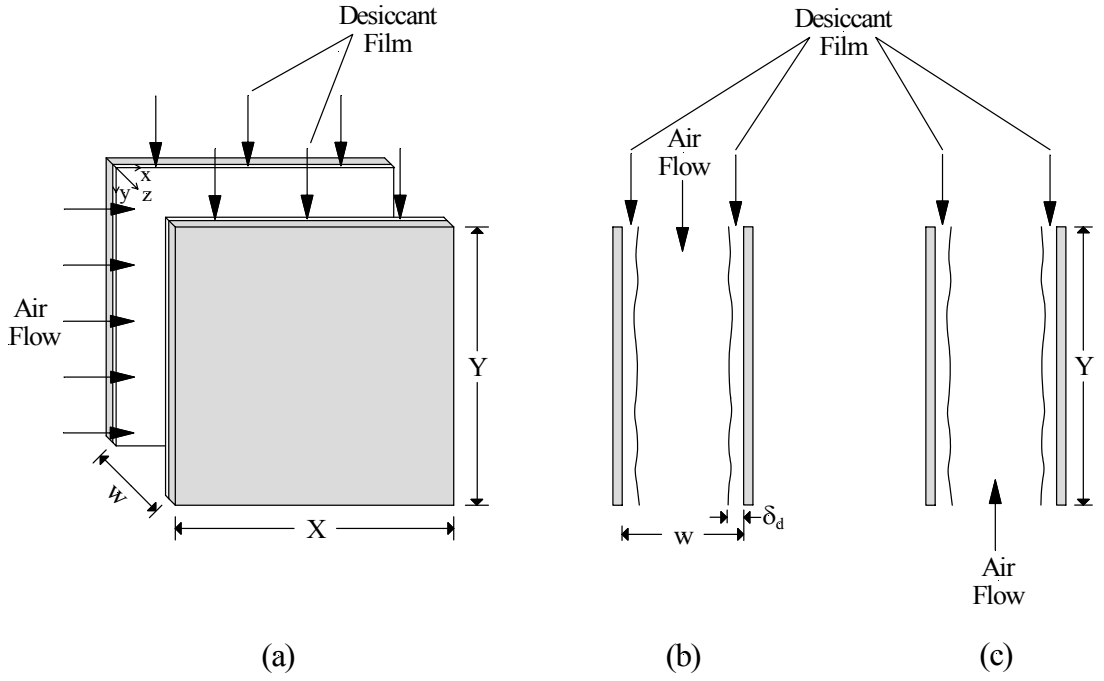

Figure 2.1 Channel schematic for (a) crossflow, (b) parallel, and (c) counterflow arrangements

To model the dehumidification process, the air flow and each desiccant film are divided into control volumes. The control volumes relative to the plate are illustrated in Figure 2.2 and separated in Figure 2.3 to include the rates of mass, water, and energy that cross the inlet and exit of the desiccant and air control volumes. Even though a parallel-flow arrangement is depicted, the direction of the air stream does not affect the governing equations for the control volume, but rather influences the procedure when analyzing the entire plate.

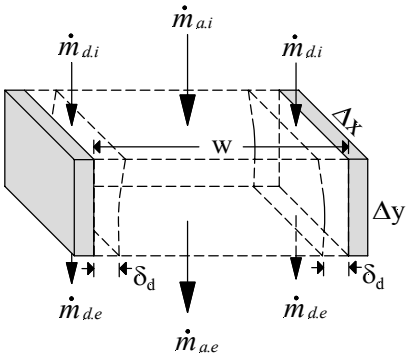

Figure 2.2 Control volume relative to the plates

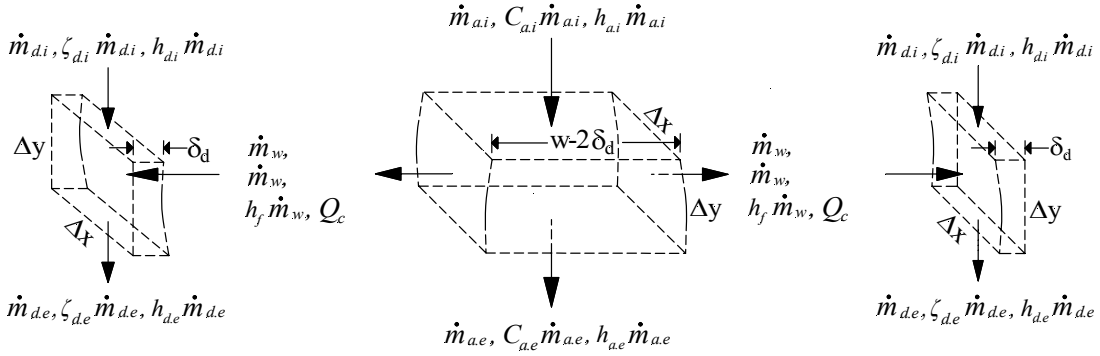

Figure 2.3 Individual control volumes for the air flow and desiccant films

For each control volume, the inlet mass flow rate, inlet concentration of water, and inlet enthalpy, determined from the inlet temperature, are known. The inlet concentration of water in the air stream, C_a (kg_w/kg_a), is calculated using the molecular weight, *MW*, of water and dry air and the respective partial pressures according to

$$C_a = \frac{MW_w P_w}{MW_{da}(P - P_w) + MW_w P_w} \tag{2.1}$$

In addition, the humidity ratio, W_a (kg_w/kg_{da}), determined from

$$W_a = \frac{MW_w P_w}{MW_{da}(P - P_w)} \tag{2.2}$$

can be used to determine the inlet concentration of water in the air stream. Combining Equations (2.2) and (2.1) gives the expression

$$C_a = \frac{W_a}{1 + W_a} \tag{2.3}$$

The inlet concentration of water in the desiccant solution, ζ_d, is related to the concentration of the desiccant in the solution, C_d, by

$$\zeta_d = 1 - C_d \tag{2.4}$$

To determine the exiting conditions for the air flow and desiccant film, control volumes conservation principles will be used. Conservation of mass will yield the exiting mass flow rates; conservation of water will yield the exiting concentration of water; and, finally, conservation of energy will be used to determine the exiting temperatures. The assumptions made in the formulation of the governing equations for one control volume are:

- Property values are constant and equal to the inlet value across the control volume
- Thermodynamic equilibrium exists at the air-desiccant interface

- Steady state
- No heat or mass is transferred to or from the surroundings
- No shear forces exists between the air and desiccant solution
- No entrance length effects
- No body forces

2.1.1 Adiabatic Absorption

For adiabatic absorption there is no internal cooling; therefore, for steady-state conditions no heat is transferred from the desiccant film to the plate. The temperature of the desiccant film and air flow will increase due the heat of absorption and a sufficient desiccant mass flow rate is needed to account for the increase in temperatures.

Referring to the control volume for the air flow in Figure 2.3, conservation of mass is

$$\dot{m}_{a.i} = \dot{m}_{a.e} + 2\dot{m}_w \tag{2.5}$$

where the mass flow rate of the air, $\dot{m}_a$, is composed of dry air and water vapor as

$$\dot{m}_a = \dot{m}_{da} + \dot{m}_{wv} \tag{2.6}$$

Similarly, conservation of mass over the control volume for a desiccant film yields

$$\dot{m}_{d.i} + \dot{m}_w = \dot{m}_{d.e} \tag{2.7}$$

Water is transferred from the air to the desiccant solution due to a difference in vapor pressure which corresponds to a difference in water concentration. The rate of water transferred to one desiccant film, $\dot{m}_w$, is determined from

$$\dot{m}_w = h_m \rho_a (C_a - C_I) \Delta x \Delta y \tag{2.8}$$

where h_m is the mass transfer coefficient in (m/s) and C_I is the equilibrium water concentration in the air at the air-desiccant interface. The equilibrium water

concentration is calculated by using the vapor pressure of the liquid desiccant solution instead of the water vapor pressure in Equation (2.1).

Next, the mass balance of water for each control volume will determine the exiting water concentration in the air and desiccant solution. The mass balance for dry air is constant across the control volume

$$\dot{m}_{da.i} = \dot{m}_{da.e} \tag{2.9}$$

Substituting Equations (2.9) and (2.6) into Equation (2.5) results in the mass balance for water vapor in the air

$$\dot{m}_{wv.i} = \dot{m}_{wv.e} + 2\dot{m}_w \tag{2.10}$$

where the mass flow rate of water vapor in the air, $\dot{m}_{wv}$, is

$$\dot{m}_{wv} = C_a \dot{m}_a \tag{2.11}$$

Using Equation (2.11), the mass balance of water in the air becomes

$$C_{a.i}\dot{m}_{a.i} = C_{a.e}\dot{m}_{a.e} + 2\dot{m}_w \tag{2.12}$$

Solving for the exiting concentration of water in the air stream results in

$$C_{a.e} = \frac{C_{a.i}\dot{m}_{a.i} - 2\dot{m}_w}{\dot{m}_{a.e}} \tag{2.13}$$

where $\dot{m}_{a.e}$ is determined from Equation (2.5). Similarly, the mass balance of water in the desiccant solution is

$$\zeta_{d.i}\dot{m}_{d.i} + \dot{m}_w = \zeta_{d.e}\dot{m}_{d.e} \tag{2.14}$$

which results in an expression for the exiting concentration of water in the desiccant film of

$$\zeta_{d.e} = \frac{\zeta_{d.i}\dot{m}_{d.i} + \dot{m}_w}{\dot{m}_{d.e}} \tag{2.15}$$

Finally, the exiting temperatures are determined from an energy balance, which for the air control volume is

$$\dot{m}_{a.i}h_{a.i} = \dot{m}_{a.e}h_{a.e} + 2\dot{m}_w h_{f.e} + 2Q_c \tag{2.16}$$

where Q_c is the convective heat transferred from the air to a desiccant film and is determined by

$$Q_c = h_h(T_a - T_d)\Delta x\Delta y \tag{2.17}$$

where h_h is the convective heat transfer coefficient in (W/m^2-K). Dividing the air into is components as expressed in Equation (2.6), the energy balance can be rewritten as

$$\dot{m}_{da.i}h_{da.i} + \dot{m}_{wv.i}h_{g.i} = \dot{m}_{da.e}h_{da.e} + \dot{m}_{wv.e}h_{g.e} + 2\dot{m}_w h_{f.e} + 2Q_c \tag{2.18}$$

Substituting in the exiting mass flow rate for dry air and water vapor, from Equation (2.9) and (2.10), respectively, gives

$$\dot{m}_{da.i}h_{da.i} + \dot{m}_{wv.i}h_{g.i} = \dot{m}_{da.i}h_{da.e} + (\dot{m}_{wv.i} - 2\dot{m}_w)h_{g.e} + 2\dot{m}_w h_{f.e} + 2Q_c \tag{2.19}$$

which can be expanded and rearrange to become

$$0 = \dot{m}_{da.i}(h_{da.e} - h_{da.i}) + \dot{m}_{wv.i}(h_{g.e} - h_{g.i}) - 2\dot{m}_w(h_{g.e} - h_{f.e}) + 2Q_c \tag{2.20}$$

In order to determine the exiting temperature of the air flow, the enthalpy values must be represented as a function of temperature. This is done using the expressions

$$h_e - h_i = c_p(T_e - T_i) \tag{2.21}$$

$$h_{f.e} = c_{p.f}T_{a.e} \tag{2.22}$$

$$h_{g.e} = h_{g.0^\circ C} + c_{p.g}T_{a.e} \tag{2.23}$$

where $h_{g.0^\circ C}$ is the enthalpy of water vapor at 0°C. Substituting Equations (2.21) through (2.23) into Equation (2.20) results in

$$0 = \dot{m}_{da.i} c_{p.da} (T_{a.e} - T_{a.i}) + \dot{m}_{wv.i} c_{p.g} (T_{a.e} - T_{a.i}) - 2\dot{m}_w (h_{g.0^\circ C} + c_{pg} T_{a.e} - c_{p.f} T_{a.e}) + 2Q_c \quad (2.24)$$

which yields the expression for the exiting air temperature

$$T_{a.e} = \frac{\dot{m}_{da.i} c_{p.da} T_{a.i} + \dot{m}_{wv.i} c_{p.g} T_{a.i} + 2\dot{m}_w h_{g.0^\circ C} - 2Q_c}{\dot{m}_{da.i} c_{p.da} + \dot{m}_{wv.i} c_{p.g} - 2\dot{m}_w (c_{p.g} - c_{p.f})} \quad (2.25)$$

Likewise, the energy balance for a desiccant film control volume is

$$\dot{m}_{d.i} h_{d.i} + \dot{m}_w h_{f.e} + Q_c = \dot{m}_{d.e} h_{d.e} \quad (2.26)$$

The enthalpy of the desiccant is unknown and taken to be equal to the specific heat time the temperature given by

$$h_d = c_{p.d} T_d \quad (2.27)$$

The energy Equation becomes

$$\dot{m}_{d.i} c_{p.d} T_{d.i} + \dot{m}_w c_{p.f} T_{a.e} + Q_c = \dot{m}_{d.e} c_{p.d} T_{d.e} \quad (2.28)$$

and the expression for the exiting desiccant temperature is

$$T_{d.e} = \frac{\dot{m}_{d.i} c_{p.d} T_{d.i} + \dot{m}_w c_{p.f} T_{a.e} + Q_c}{\dot{m}_{d.e} c_{p.d}} \quad (2.29)$$

2.1.2 Isothermal Absorption

During isothermal absorption each plate is internally cooled with water or a refrigerant. With an adequate flow rate of the internal fluid, the desiccant plate and, therefore, the desiccant solution, will have a constant temperature equal to that of the fluid within a negligible distance of the absorber inlet.

Differences from the adiabatic case arise in the energy balances because the heat of absorption is effectively removed by the internal cooling and, thus, can be neglected from Equation (2.20), which results in

$$0 = \dot{m}_{da.i}(h_{da.e} - h_{da.i}) + \dot{m}_{wv.i}(h_{g.e} - h_{g.i}) + 2Q_c \tag{2.30}$$

Using the same expression for the change in enthalpy, Equation (2.21), the exiting air temperature becomes

$$T_{a.e} = \frac{\dot{m}_{da.i}c_{p.da}T_{a.i} + \dot{m}_{wv.i}c_{p.g}T_{a.i} - 2Q_c}{\dot{m}_{da.i}c_{p.da} + \dot{m}_{wv.i}c_{p.g}} \tag{2.31}$$

which reduces to

$$T_{a.e} = T_{a.i} - \frac{2Q_c}{\dot{m}_{a.i}c_{p.a}} \tag{2.32}$$

2.1.3 Determination of Transfer Coefficients

In the process of finding the exiting conditions for the air flow and desiccant film the heat and mass transfer coefficients must be known. For laminar flow through a duct with constant surface temperature, the Nusselt number for air is 7.54. The heat transfer coefficient can then be obtained from the definition of Nusselt number

$$h_h = \frac{Nu * k_a}{D_h} \tag{2.33}$$

where k_a is the thermal conductivity of air and the hydraulic diameter, D_h, is

$$D_h = \frac{4 * A_c}{P_{wetted}} = \frac{4Y * (w - 2\delta_d)}{2Y} = 2(w - 2\delta_d) \tag{2.34}$$

with δ_d, the thickness of the desiccant film reported by Rahamah et al. (1997) to be

$$\delta_d = \left(\frac{3\dot{m}_d \mu_d}{\rho_d^2 g} \right)^{1/3} \tag{2.35}$$

where v is the viscosity, ρ the density, and g the acceleration due to gravity. The mass transfer coefficient is determined from the Chilton-Coulburn analogy as

$$h_m = \frac{h_h}{c_{p.a}} \left(\frac{\alpha_a}{D_{a.wv}} \right)^{-2/3} \tag{2.36}$$

were α is the thermal diffusivity and D is the mass diffusivity. For each control volume δ_d, D_h, h_h , h_m , and the physical properties are recalculated based on the inlet conditions of the control volume.

2.2 Model Procedure

2.2.1 Parallel Flow

The procedure for determining the absorber output conditions from the control volumes depends on the flow arrangement. For the simplest case of a parallel-flow arrangement, Figure 2.1 (b), the width of each control volume is equal to the width of the plate. The height of each control volume is the height of the plate divided by the number of control volumes, *Ny*, as shown in Figure 2.4.

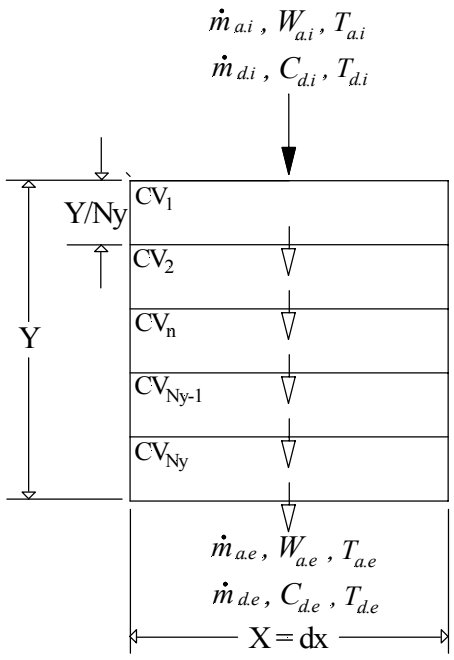

Figure 2.4 Procedure illustration for parallel flow

The known absorber inlet conditions for the air and desiccant solution are the inputs to the first control volume. The outputs of this control volume are determined as described in Section 2.1 and become the inlet conditions for the next control volume. This process is repeated according to the flow chart in Figure 2.5 until the outputs for the final control volume, the exiting conditions of the absorber, are determined.

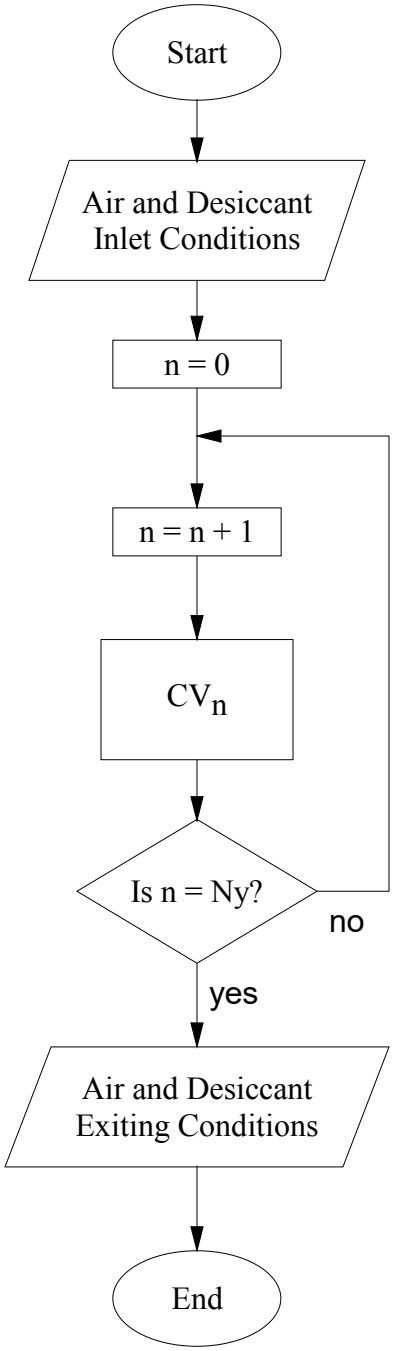

Figure 2.5 Flow chart to determine the exiting conditions of the absorber for parallel flow

2.2.2 Counterflow

Complexities arise in the counterflow arrangement, Figure 2.1 (c), because an iterative approach is required. Initially, the desiccant solution has a constant concentration and temperature equal to the inlet conditions of the absorber for every control volume, displayed in Figure 2.6 (a). The outlet air conditions are determined and the transfer rates of water and heat from each control volume are saved. The latter information is then used to determine the exiting desiccant conditions, Figure 2.6 (b). Next, the calculated desiccant outputs for each control volume replace the previously constant desiccant values and the exiting air conditions are recalculated. This process, outlined in Figure 2.7, continues until two consecutive solutions are within a specified tolerance.

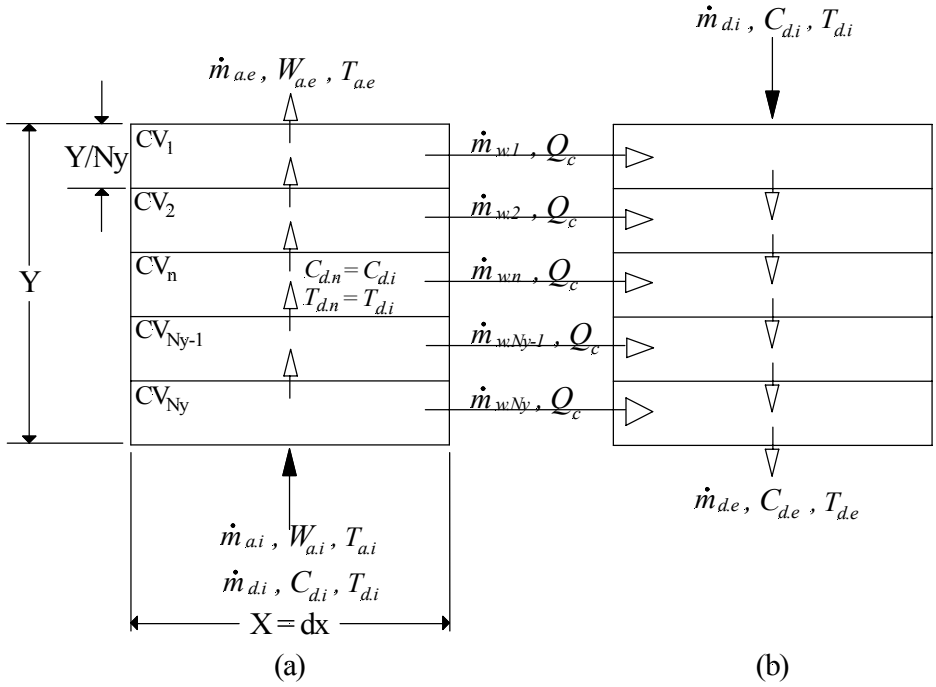

Figure 2.6 Procedure illustration for counterflow

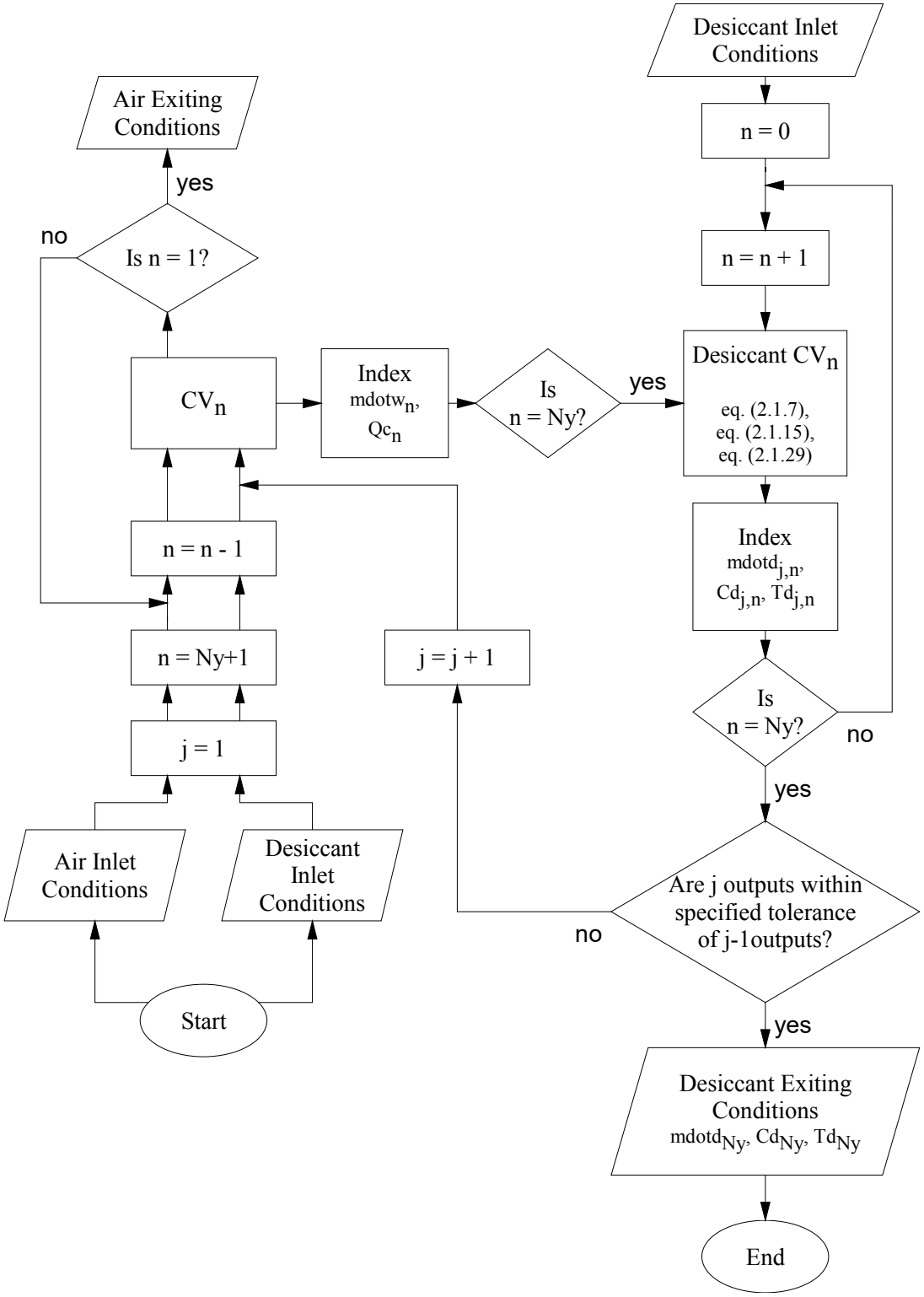

Figure 2.7 Flow chart to determine the exiting conditions of the absorber for counterflow

2.2.3 Crossflow

In the previous two arrangements, parallel and counterflow, the program procedure was one dimensional. In the crossflow arrangement, Figure 2.1 (a), the procedure, outlined in Figure 2.9, becomes two dimensional. The height of each control volume remains the height divided by the number of control volumes down the plate, *Ny*. The width of each control volume becomes the width of the plate divided by the number of control volumes across the plate, *Nx*, given in Figure 2.8.

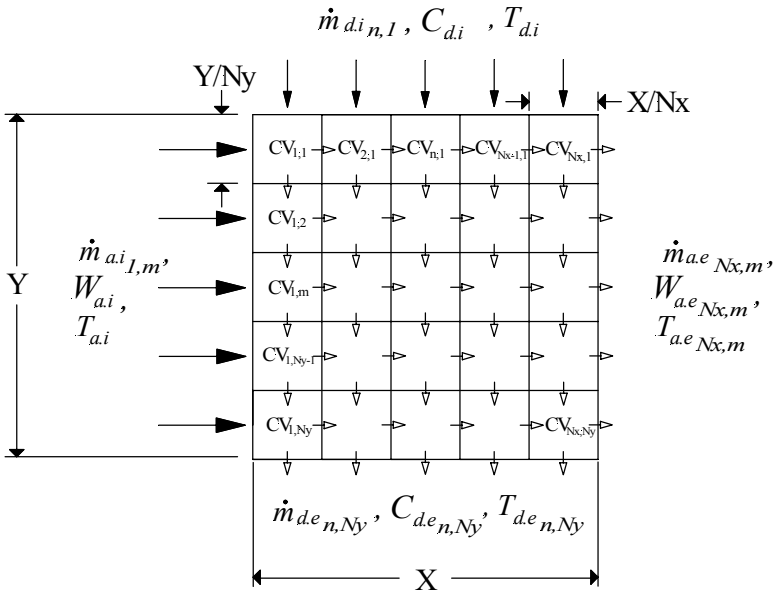

Figure 2.8 Procedure illustration for crossflow

An important note is the inlet flow rates to the absorber must be adjusted to obtain the inlet mass flow rate for the control volume. The inlet mass flow rate of air for the control volumes in the first column, $\dot{m}_{a.i_{1,m}}$ for $CV_{1,m}$, is

$$\dot{m}_{a.i_{1,m}} = \frac{\dot{m}_{a.i}}{Ny} \tag{2.37}$$

and the inlet desiccant mass flow rate for the control volumes in the first horizontal row, $\dot{m}_{d_{n,1}}$ for $CV_{n,1}$, is

$$\dot{m}_{d_{n,1}} = \frac{\dot{m}_{d.i}}{Nx} \tag{2.38}$$

To determine the exiting mass flow rates leaving the absorber, the individual rates leaving the control volumes are summed. For example, the exiting desiccant mass flow rate of the absorber is

$$\dot{m}_{d.e} = \sum_{n=1}^{Nx} \dot{m}_{d.e_{n,Ny}} \tag{2.39}$$

To quantify the other exiting conditions, an average is taken of the exiting values from the control volumes on the last row or column. For example, the exiting humidity ratio of air is

$$W_{a.e} = \frac{1}{Ny} \sum_{m=1}^{Ny} W_{a.e_{Nx,m}} \tag{2.40}$$

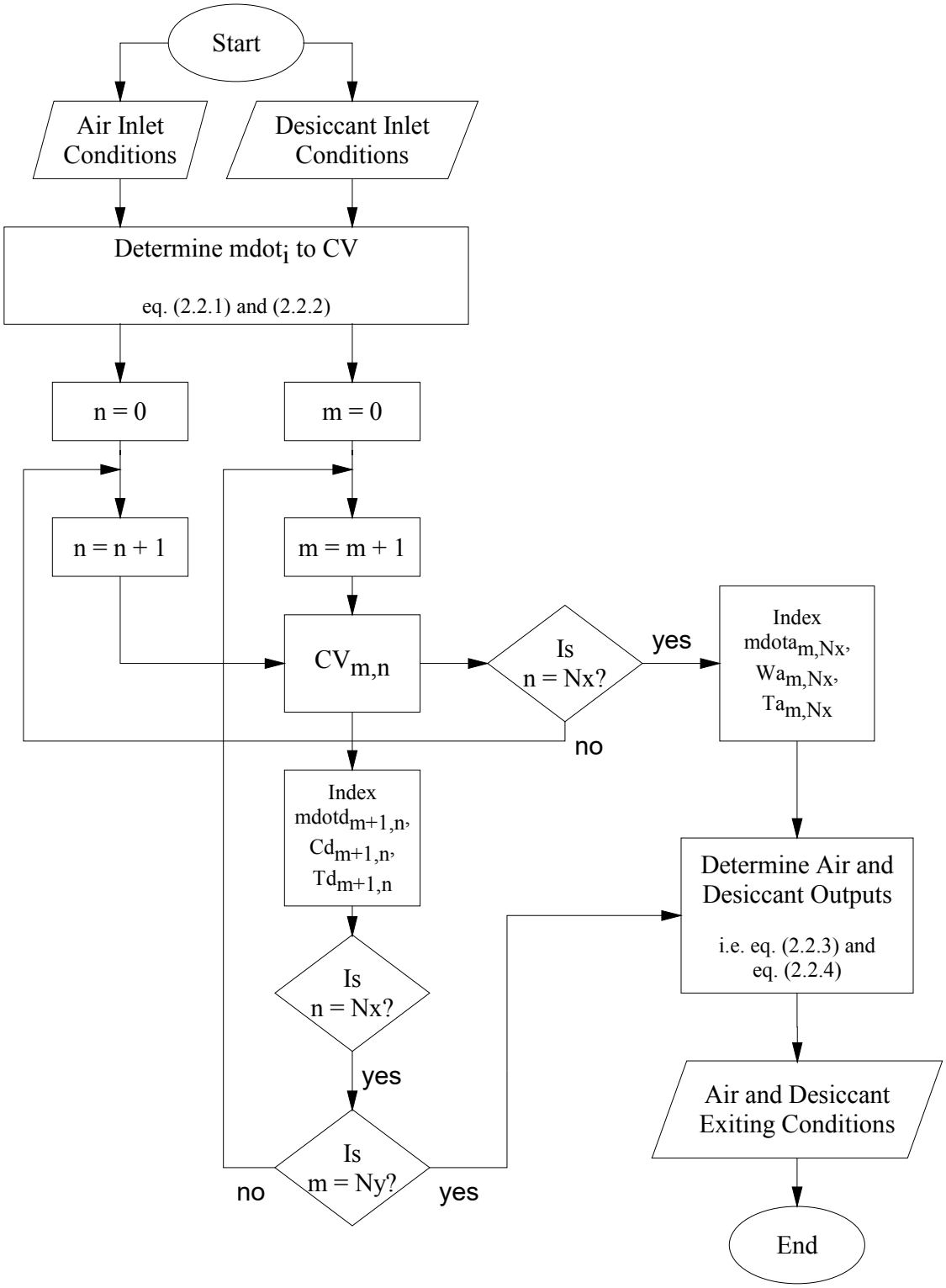

Figure 2.9 Flow chart to determine exiting conditions of the absorber for crossflow

CHAPTER 3

RESULTS AND DISCUSSION

To initially validate the results of the program, a simple mass balance was performed to verify that the amount of water lost by the air was equal to the amount of water absorbed by the two desiccant films. This is represented by

$$\dot{m}_{a.i} C_{a.i} - \dot{m}_{a.e} C_{a.e} = 2(\dot{m}_{d.e} \zeta_{d.e} - \dot{m}_{d.i} \zeta_{d.i}) \tag{3.1}$$

Next, the model was compared to data from literature. The parallel-flow arrangement was compared to the variable-thickness model developed by Mesquita et al. (2006) which used the constant property values given in Table 3.1 in determining the exiting air temperature and humidity ratio for a range of inlet desiccant mass flow rates. The inlet conditions and absorber characteristics for the model are given in Table 3.2. As shown in Table 3.3 and Figure 3.1, the results of the present model are in good agreement with the variable-thickness model developed by Mesquita et al. (2006) with the maximum error being about 5%.

Table 3.1 Constant property values used by Mesquita et al. (2006)

	Air	LiCl
k (W/m-K)	0.0275	0.558
c_p (J/kg-K)	990	3140
ρ (kg/m^3)	1.11	1394
μ (kg/m-s)	1.90E-05	1.86E-03
D (m^2/s)	2.65E-05	1.20E-09

Table 3.2 Inlet conditions and absorber characteristics used to compare the present model with the variable-thickness model by Mesquita et al. (2006)

	Air	LiCl
$\dot{m}$ (kg/s)	0.01264	
W_a (kg$_w$/kg$_a$)	0.015228	
C_d (kg$_d$/kg$_s$)		0.4
T (°C)	30	25
Y (m)	0.5	
X (m)	1	
w (m)	0.005	
Ny	500	
Desiccant	LiCl	
Flow Arrangement	Parallel	
Absorption Process	Isothermal	
T_{wall} (°C)	25	

Table 3.3 Results of the present model and the variable-thickness model by Mesquita et al. (2006)

	Present		Mesquita et at. (2006) Variable-Thickness		Error	
$\dot{m}_{d.i}$ (kg/s)	$T_{a.e}$ (°C)	$W_{a.e}$ (g/kg)	$T_{a.e}$ (°C)	$W_{a.e}$ (g/kg)	$T_{a.e}$ (°C)	$W_{a.e}$ (g/kg)
$\dot{m}_{a.i}$	25.90	5.99	25.87	5.86	0.12%	2.15%
$\dot{m}_{a.i}$ /2.5	25.95	6.16	25.86	5.97	0.35%	3.18%
$\dot{m}_{a.i}$ /5	25.98	6.32	25.86	6.11	0.47%	3.42%
$\dot{m}_{a.i}$ /10	26.00	6.56	25.86	6.36	0.56%	3.13%
$\dot{m}_{a.i}$ /20	26.02	6.96	25.86	6.81	0.63%	2.29%
$\dot{m}_{a.i}$ /30	26.03	7.32	25.86	7.20	0.67%	1.58%
$\dot{m}_{a.i}$ /40	26.04	7.64	25.86	7.56	0.69%	1.04%
$\dot{m}_{a.i}$ /50	26.04	7.93	25.86	7.87	0.71%	0.71%
$\dot{m}_{a.i}$ /60	26.05	8.20	25.86	8.16	0.73%	0.49%
$\dot{m}_{a.i}$ /70	26.05	8.45	25.86	8.41	0.74%	0.41%
$\dot{m}_{a.i}$ /80	26.05	8.68	25.86	8.64	0.75%	0.37%
$\dot{m}_{a.i}$ /90	26.06	8.89	25.86	8.86	0.75%	0.38%
$\dot{m}_{a.i}$ /100	26.06	9.09	25.86	9.06	0.76%	0.34%
$\dot{m}_{a.i}$ /150	26.06	9.93	25.86	9.83	0.79%	1.02%
$\dot{m}_{a.i}$ /200	26.07	10.56	25.86	10.41	0.80%	1.43%
$\dot{m}_{a.i}$ /250	26.07	11.05	25.87	10.82	0.77%	2.16%
$\dot{m}_{a.i}$ /300	26.07	11.45	25.87	11.12	0.78%	2.91%
$\dot{m}_{a\ i}$ /350	26.07	11.77	25.87	11.33	0.78%	3.95%
$\dot{m}_{a.i}$ /400	26.07	12.05	25.87	11.53	0.79%	4.48%

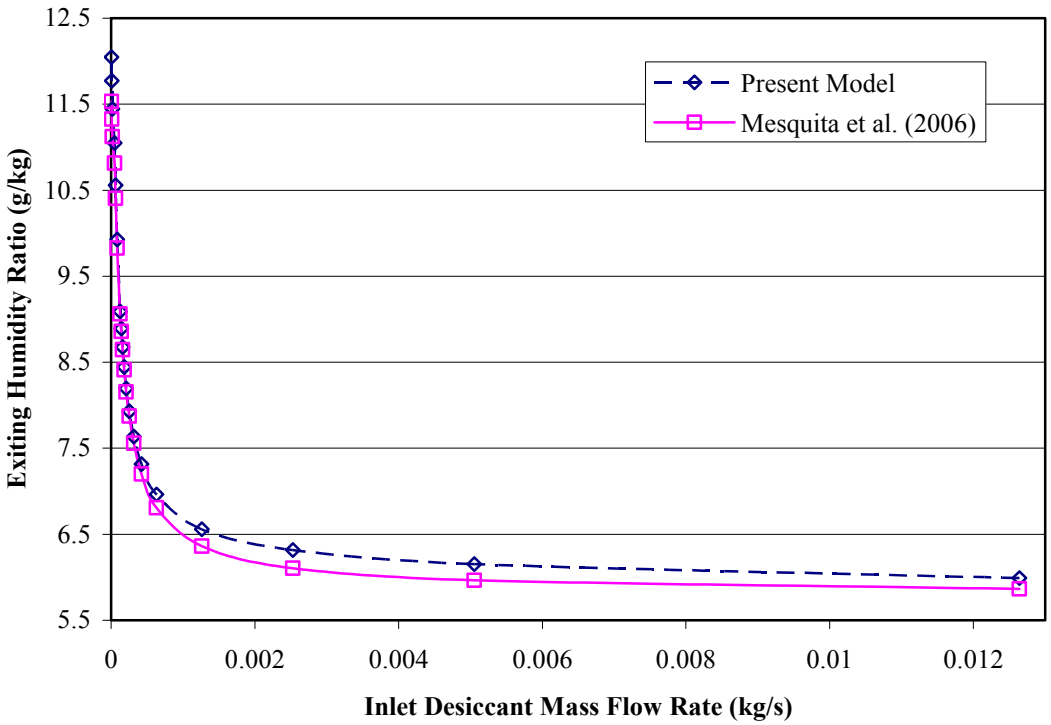

Figure 3.1 Exiting humidity ratio for a range of inlet desiccant mass flow rates of the present model compared to the variable-thickness model by Mesquita et al. (2006)

An investigation was done to determine the effect of using the constant property values reported in Table 3.1 in the present model. There was a maximum deviation of 1.6% for the highest desiccant mass flow rate proving negligible differences when assuming constant property values under isothermal, parallel-flow arrangements.

A simulation implementing a counterflow arrangement was compared to the two sets of experiments conducted by Kessling et al. (1998b) with the absorber characteristics given in Table 3.4. The first set of experiments tested a range of inlet desiccant mass flow rates for a constant inlet air mass flow rate, and the second set used a range of inlet air mass flow rates for a constant inlet desiccant mass flow rate. Kessling et al. (1998b)

used the experimental input and output data to determine a mass transfer coefficient, β, from an iterative differential model. In an additional simulation, the present model used the β values as a constant input value for the mass transfer coefficient. The experimental inlet conditions, along with the calculated β values, for the constant inlet air mass flow rate and constant inlet desiccant mass flow rate experiments are given in Table 3.5 and 3.6, respectively. The desiccant mass flow rates presented by Kessling et al. (1998b) were for one channel of an absorber. The desiccant mass flow rates currently reported have been adjusted to reflect the mass flow rate down a single plate. In addition, the wall temperatures currently reported are an average of the measured inlet and exiting temperatures of the internal cooling water.

Table 3.4 Absorber characteristics from Kessling et al. (1998b)

Y (m)	0.46
X (m)	0.98
w (m)	0.0055
P (Pa)	96000
Flow Arrangement	Counterflow
Absorption Process	Isothermal

Table 3.5 Inlet conditions for a range of inlet desiccant mass flow rates with a constant inlet air mass flow rate of 12.64 g/s [Kessling et al. (1998b)]

$\dot{m}_d$	(g/s)	1.242	0.653	0.374	0.229	0.169	0.142	0.116
C_d	(%)	40.2	40.2	40.2	40.2	40.2	40.2	40.2
W_a	(g/kg)	14.4	14.5	14.5	14.5	14.5	14.5	14.4
T_a	(°C)	24.5	24.8	24.6	24.4	24.4	24.1	23.9
$T_{wall} = T_d$	(°C)	24.3	24.3	24.3	24.25	24.25	24.25	24.2
β	(mm/s)	25.9	25.2	22.6	20.8	20.3	21.5	20.7

Table 3.6 Inlet conditions for a range of inlet air mass flow rates with a constant inlet desiccant mass flow rate of 0.1175 g/s [Kessling et al. (1998b)]

$\dot{m}_a$	(g/s)	6.36	9.48	12.51	15.52	18.68	21.72	24.83
C_d	(%)	40.2	40.2	40.2	40.2	40.2	40.2	40.2
W_a	(g/kg)	14.5	14.4	14.6	14.6	14.7	14.7	14.7
T_a	(°C)	24.7	23.4	23.6	23.4	23.3	23.5	23.8
$T_{wall} = T_d$	(°C)	24.2	24.25	24.2	24.25	24.25	24.25	24.25
β	(mm/s)	18.7	21.5	23.5	25.4	27.7	29	30.7

Table 3.7 gives the results of the exiting humidity ratio and air temperature for the two simulations along with the experimental data for a constant air mass flow rate. The exiting humidity ratio values are plotted in Figure 3.2 for the range of inlet desiccant mass flow rates. Similarly, Table 3.8 and Figure 3.3 present the results for the range of inlet air mass flow rates.

Table 3.7 Exiting humidity ratio and air temperature results of the present model and experiments by Kessling et al. (1998b) for a range of inlet desiccant mass flow rates

	$W_{a.e}$ (g/kg)			**$W_{a.e}$ Error Kessling vs.**		**$T_{a.e}$ (°C)**			**$T_{a.e}$ Error Kessling vs.**	
$\dot{m}_{d.i}$ (g/s)	**Kessling et al. (1998)**	**Present Model**	**Present Model ($h_m = \beta$)**	**Present Model**	**Present Model ($h_m = \beta$)**	**Kessling et al. (1998)**	**Present Model**	**Present Model ($h_m = \beta$)**	**Present Model**	**Present Model ($h_m = \beta$)**
0.6210	5.3	7.0	5.8	31.6%	9.3%	25.4	24.4	24.4	4.1%	4.1%
0.3265	5.7	7.3	6.1	27.3%	7.5%	25.6	24.4	24.4	4.5%	4.5%
0.1870	6.4	7.6	6.8	19.3%	7.0%	25.5	24.4	24.4	4.4%	4.4%
0.1145	7.2	8.2	7.7	13.2%	6.4%	25.4	24.3	24.3	4.4%	4.4%
0.0845	7.8	8.6	8.2	10.3%	5.6%	25.4	24.3	24.3	4.4%	4.4%
0.0710	8.0	8.9	8.5	11.4%	6.0%	25.3	24.2	24.2	4.3%	4.3%
0.0580	8.5	9.3	9.0	8.9%	5.6%	25.3	24.1	24.1	4.7%	4.7%

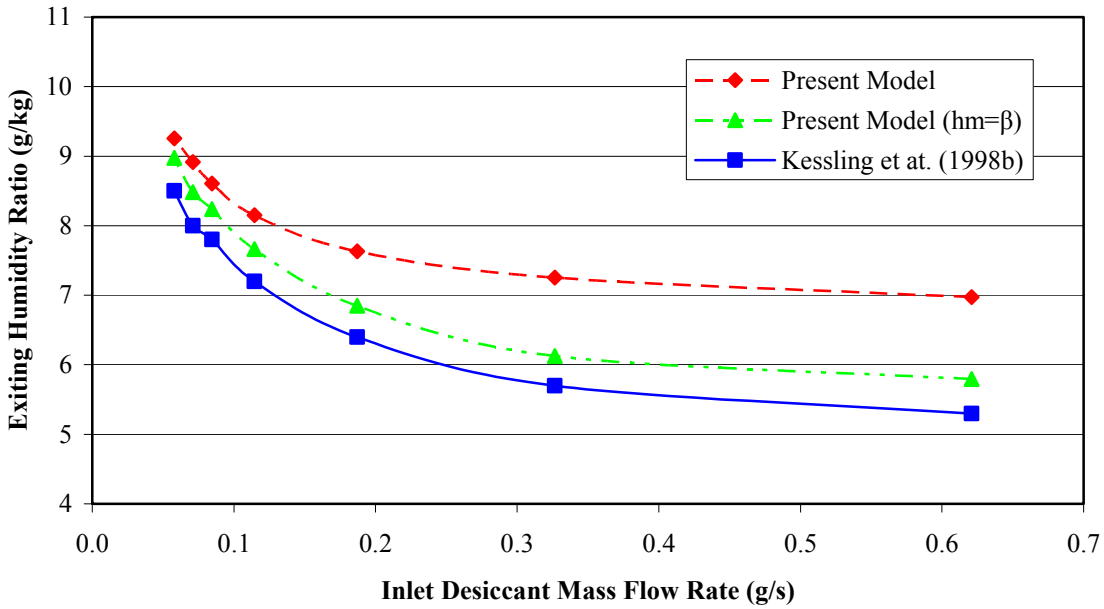

Figure 3.2 Exiting humidity ratio for a range of inlet desiccant mass flow rates of the present model compared to experimental data by Kessling et al. (1998b)

Table 3.8 Exiting humidity ratio and air temperature results of the present model and experiments by Kessling et al. (1998b) for a range of inlet air mass flow rates

	$W_{a.e}$ (g/kg)			$W_{a.e}$ Error Kessling vs.		$T_{a.e}$ (°C)			$T_{a.e}$ Error Kessling vs.	
$\dot{m}_{a.i}$ (g/s)	Kessling et al. (1998b)	Present Model	Present Model ($h_m=\beta$)	Present Model	Present Model ($h_m=\beta$)	Kessling et al. (1998b)	Present Model	Present Model ($h_m=\beta$)	Present Model	Present Model ($h_m=\beta$)
6.36	4.7	5.5	5.3	16.6%	13.4%	25.3	24.2	24.2	4.2%	4.2%
9.48	5.9	6.9	6.3	17.2%	7.4%	25.8	1.0	24.1	96.1%	6.6%
12.51	7.0	8.1	7.3	15.8%	3.8%	26.3	24.0	24.0	8.6%	8.6%
15.52	7.8	9.0	8.0	15.4%	2.5%	26.5	23.9	23.9	9.6%	9.6%
18.68	8.5	9.8	8.6	14.9%	1.3%	26.6	23.8	23.8	10.4%	10.4%
21.72	9.1	10.3	9.1	13.4%	0.3%	26.8	23.9	23.9	10.9%	10.9%
24.83	9.5	10.8	9.5	13.5%	0.4%	26.9	24.0	24.0	10.7%	10.7%

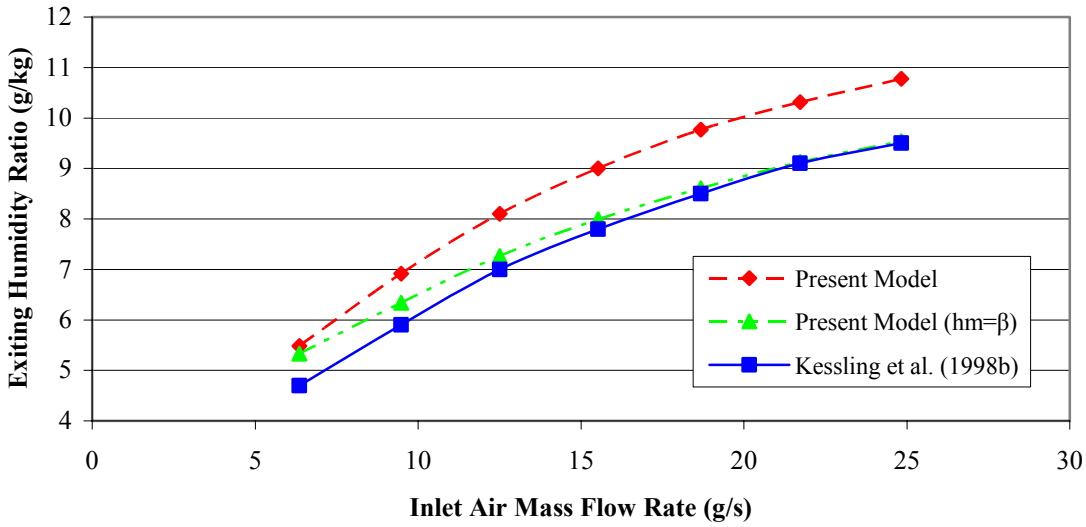

Figure 3.3 Exiting humidity ratio for a range of inlet air mass flow rates of the present model compared to experimental data by Kessling et al. (1998b)

The two models follow the experimental trend for both sets of experiments. For constant inlet air mass flow rates the present model showed large errors, up to 30%, for high inlet desiccant mass flow rates. When Mesquita et al. (2006) compared a counterflow arrangement of the variable-thickness model to this set of experiments, the error in the exiting humidity ratio went from 0% for low desiccant mass flow rate to about 15% for high desiccant mass flow rate. The difference between the present model and the variable-thickness model by Mesquita et al. (2006) could be due to use of the constant Number along with the method used for determining the mass transfer coefficient. For the constant inlet desiccant mass flow rate the present model predicted the exiting air conditions within a reasonable margin of error between about 13% and 16%.

When comparing to both sets of experiments, the present model consistently underpredicted the dehumidification; however, when the β values were used as the mass transfer coefficients in the model, the results were significantly improved. For high inlet desiccant mass flow the error was just over 9%. Varying the inlet air mass flow rate resulted in errors of about 13.5% for low mass flow rates to almost 0% for high mass flow rates.

CHAPTER 4

UNCERTAINTY AND VALIDATION

4.1 Uncertainty

The model uncertainty was determined using the uncertainty propagation equation published in Coleman and Steele (1999).

$$\frac{U_m}{m} = \left[\left(\frac{Y_1}{m} \frac{\partial m}{\partial Y_1} \right)^2 \left(\frac{U_{Y_1}}{Y_1} \right)^2 + \left(\frac{Y_2}{m} \frac{\partial m}{\partial Y_2} \right)^2 \left(\frac{U_{Y_2}}{Y_2} \right)^2 + \ldots + \left(\frac{Y_J}{m} \frac{\partial m}{\partial Y_J} \right)^2 \left(\frac{U_{Y_J}}{Y_J} \right)^2 \right]^{0.5} \tag{4.1}$$

where

m = model result of interest

U_m = model uncertainty

Y_j = inlet parameter

U_{Y_j} = inlet parameter uncertainty

and the derivative term was numerically approximated using a first-order differential operator according to

$$\frac{\partial m}{\partial Y_j} = \lim_{\Delta Y_j \to 0} \frac{m(Y_j + \Delta Y_j) - m(Y_j)}{\Delta Y_j} \tag{4.2}$$

The nominal model inlet values and associated uncertainties, given in Table 4.1, were taken from a single experiment in Kessling et al. (1998b), with the exception of the absorber dimension uncertainties, which were estimated; the Nusselt number, which only

applied to the model; and Nusselt number uncertainty, which was estimated. The resulting uncertainty of the exiting humidity ratio was found to be 7.8%.

Table 4.1 Nominal values and uncertainties of inlet conditions

Input Parameter	Nominal Value	Uncertainty
$\dot{m}_a$ (kg/s)	0.01264	0.0002
W_a (kg/kg)	0.0145	0.0002
T_a (°C)	24.4	0.5
$\dot{m}_d$ (kg/s)	0.0001145	4.0E-6
ϕ_d (%)	0.402	0.002
T_d (°C)	24.25	0.1
T_w (°C)	24.25	0.1
Nu	7.541	1.5
Y (m)	0.46	0.001
X (m)	0.98	0.001
w (m)	0.0055	0.0005

In addition, the uncertainty magnification factor, *UMF*, and the uncertainty percentage contribution, *UPC*, are two important factors that influence the model uncertainty. The *UMF* indicates the influence of the uncertainty in the inlet parameter, U_{Y_j}, on the model uncertainty and is defined as

$$UMF_j = \frac{Y_j}{m}\frac{\partial m}{\partial Y_j} \tag{4.3}$$

The *UPC* is the percent contribution each inlet parameter has on the model uncertainty and is determined according to

$$UPC = \frac{\left(\frac{\partial m}{\partial Y_j}\right)^2 U_{Y_j}^2}{U_m^2} = \frac{UMF^2\left(\frac{U_{Y_j}}{Y_j}\right)^2}{\left(\frac{U_m}{m}\right)^2} \tag{4.4}$$

The *UMF* and *UPC* values for the inlet conditions are presented in Table 4.2. The *UPC* of the Nusselt number is significantly higher than the other input variables. This indicates that the Nusselt number contributes to most, 79%, of the uncertainty value of the exiting humidity ratio. All the *UPC* values along with the *UMF* values are compared in Figure 4.1.

Table 4.2 *UMF* and *UPC* values of the inlet parameters

Inlet Parameter	*UMF*	*UPC*
$\dot{m}_a$ (kg/s)	0.51	0.95%
W_a (kg/kg)	0.66	1.35%
T_a (°C)	-0.02	0.00%
$\dot{m}_d$ (kg/s)	-0.16	0.51%
W_d (kg/kg)	-1.24	0.61%
T_d (°C)	0.00	0.00%
T_w (°C)	0.74	0.15%
Nu	-0.35	79.21%
Y (m)	-0.35	0.01%
X (m)	-0.35	0.00%
w (m)	0.36	17.20%

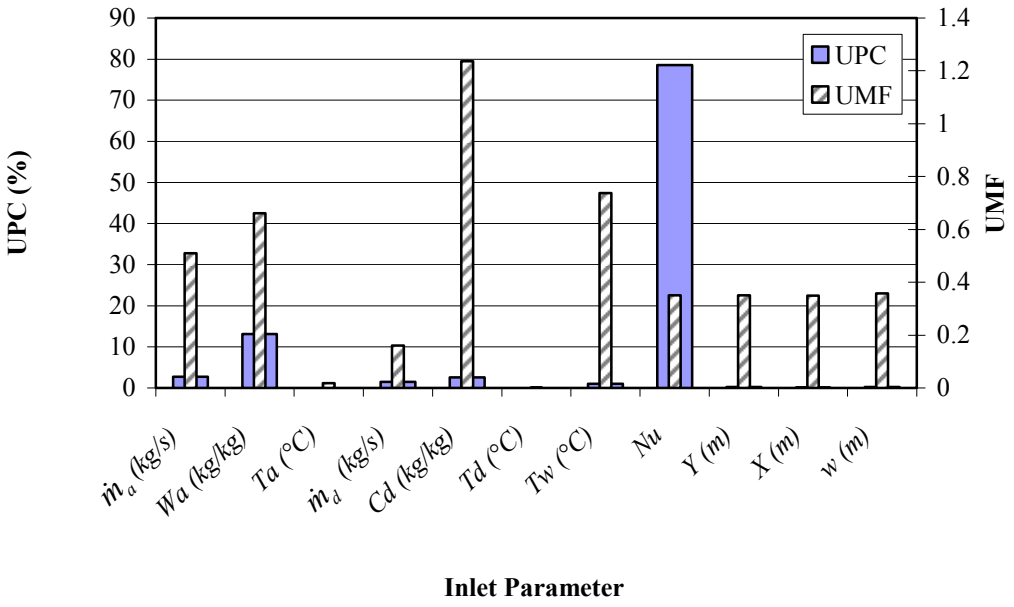

Figure 4.1 Comparison of the *UPC* and *UMF* values of the input parameters

Since the uncertainty associated with the Nusselt number was estimated, the UPC values and relative uncertainty in the exiting humidity ratio were determined for Nusselt number uncertainties ranging from 2.5% to 30%. The results, displayed in Figure 4.2, demonstrate the dependence of the uncertainty in exiting humidity ratio on the Nusselt number uncertainty. The *UPC* ranges from about 6% to 90% with the humidity ratio uncertainty ranging from about 4% to 11%.

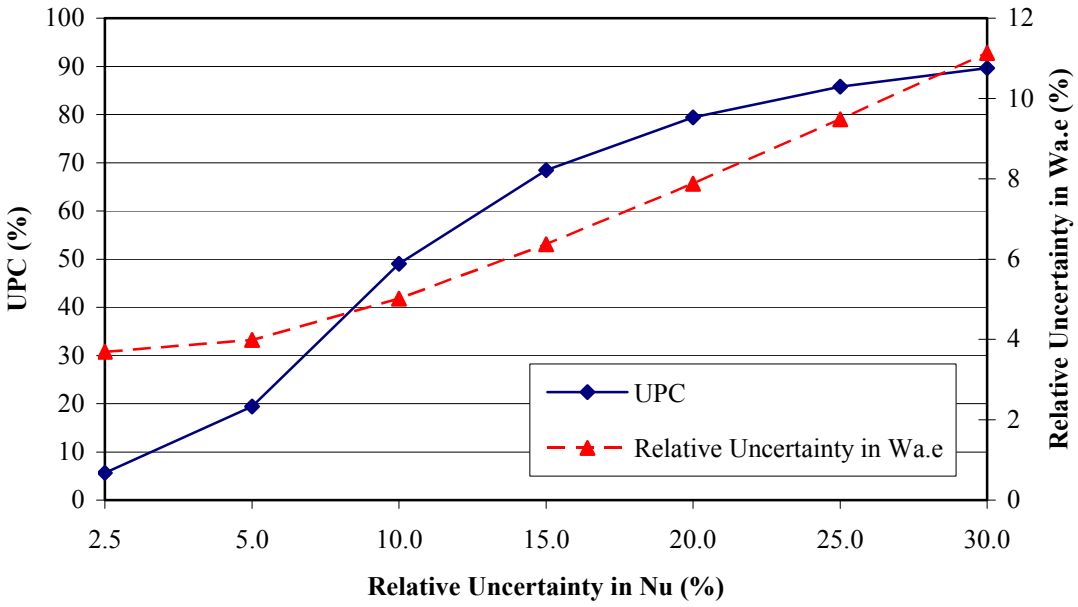

Figure 4.2 *UPC* and relative uncertainty of the exiting humidity ratio for a range of relative Nusselt number uncertainties.

Finally, a study was done to determine the uncertainty in the model predictions of the experiments conducted by Kessling et al. (1998b) using the β values as model inputs. The nominal values, given in Figures 3.5 and 3.6, for constant inlet mass flow rate and constant desiccant mass flow rate, respectively, with the associated uncertainties given in Table 4.1. The model results and associated uncertainty range are plotted with the experimental data and its uncertainty band in Figure 4.3 and 4.4 for the constant inlet air mass flow rate and constant desiccant mass flow rate experiments, respectively. These plots show that the uncertainty ranges of the model results and experimental results for both sets of experiments overlap.

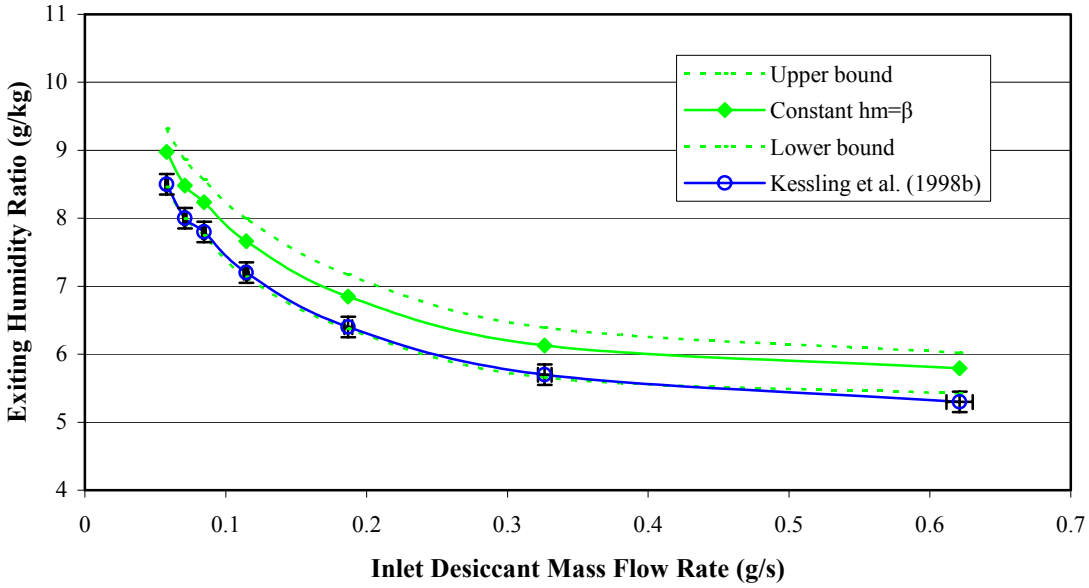

Figure 4.3 Comparison of model and experimental results with uncertainty bands for a constant inlet air mass flow rate

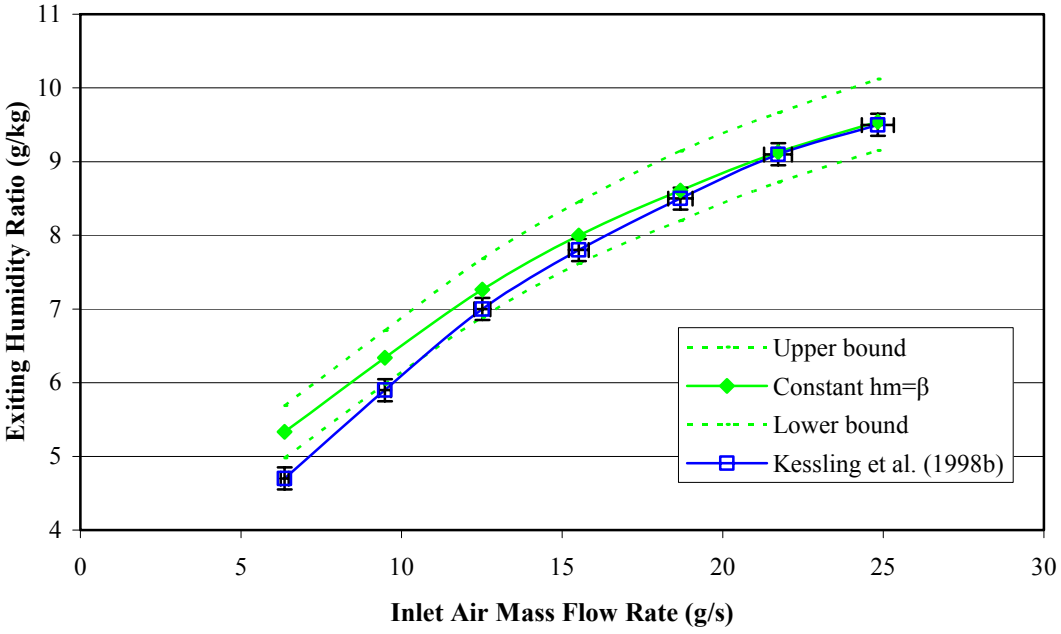

Figure 4.4 Comparison of model and experimental results with uncertainty bands for constant inlet desiccant mass flow rate

4.2 Validation

The validation of the model, m, with respect to experimental data, d, is determined by comparing the comparison error, E, to its associated uncertainty, U_E. The comparison error, which is the resultant of all the errors associated with the experimental data and the errors associated with the simulation model, is defined as [Coleman and Steele (1999)]

$$E = d - m \tag{4.1}$$

and its associated uncertainty, or the validation uncertainty, is defined as

$$U_E = \sqrt{U_d^2 + U_m^2} \tag{4.2}$$

If $|E|$ is less than U_E, the model is validated at the U_E level. If U_E is less than $|E|$, the model is validated at the $|E|$ level. However, if $|E|$ is much larger than U_E the model is not validated and there is probably justification for improving the model [Coleman and Stern (1997)].

The present model, which used the β values for the mass transfer coefficient, was compared to the experimental data from Kessling et al. (1998b). For varying inlet desiccant mass flow rates validation was achieved at the level of 8.5% and for varying inlet air mass flow rates validation was achieved at the level of 11%.

CHAPTER 5

CONCLUSION

A simplified model to determine the air and desiccant exiting conditions of a parallel-plate absorber was successfully developed. Conservation of mass, water, and energy were used in a control volume approach that allowed for property variations and varying desiccant thickness. Procedures for parallel, crossflow, and counterflow were presented. Using a constant Nusselt number proved accurate results, within 5%, of a more complicated model for flow in a parallel arrangement. However, larger errors, between 9% and 30%, arose when the model was compared to available experimental data for a counterflow arrangement. The inherent uncertainty in the Nusselt number was shown to have the most effect on the uncertainty of the exiting humidity ratio. When an experimentally determined mass transfer coefficient was used in the model, the counterflow results were within 13.5% and the associated uncertainty range fell within the uncertainty band of the experimental data. In addition, the model using the experimentally determined mass transfer coefficient was validated at the level of 8.5% for varying inlet desiccant mass flow rates and 11% for varying inlet air mass flow rates.

BIBLIOGRAPHY

ASHRAE. Handbook Fundamentals. American Society of Heating, Refrigeration and Air-Conditioning Engineers, Inc., 2005.

Ali, A., Vafai, K., Khaled, A.-R. A. 2003. "Comparative study between parallel and counter flow configurations between air and falling film desiccant in the presence of nanoparticle suspensions." International Journal of Energy Research, 27: 725-745.

Ali, A., Vafai, K., Khaled, A.-R. A. 2004. "Analysis of heat and mass transfer between air and falling film in a cross flow configuration." International Journal of Heat and Mass Transfer, 47: 743-755.

Coleman, H.W. and Steele, W.G. 1999. Experimentation and Uncertainty Analysis for Engineers (2^{nd} ed). Wiley: New York, NY.

Coleman, H.W. and Stern, F. 1997. "Uncertainties in CFD validation." Journal of Fluids Engineering, ASME 119: 795-803.

Department of Energy. Thermally Activated Technologies. 2006. Accessed Oct 2007. <http://www.eere.energy.gov/de/thermally_activated/tech_basics.html>

Fumo, N. and Goswami, D.Y. 2002. "Study of an aqueous lithium chloride desiccant system: air dehumidification and desiccant regeneration." Solar Energy, 72 (4): 351-361.

Jain, S. and Bansal, P.K. 2007. "Performance analysis of liquid desiccant dehumidification systems." International Journal of Refrigeration, 30 (7): 1117-1292.

Kessling, W., Laevemann, E., and Kapfhammer, C. 1998b. "Energy storage for desiccant cooling systems component development." Solar Energy, 64 (4-6): 209-221.

Kessling, W., Laevemann, E., and Peltzer, M. 1998a. "Energy storage in open cycle liquid desiccant cooling systems." International Journal of Refrigeration, 21 (2): 150-156.

LabVIEW 8.2, 2006. National Instruments, Austin, Texas.

Löf, G.O.G. 1955. "Cooling with solar energy in 1995 Congress on Solar Energy," Tuscon: 171-189.

Lowenstein, A., Slayzak, S., and Kozubal, E. 2006. "A zero carryover liquid-desiccant air conditioner for solar applications in 2006 National Solar Conference," Denver.

Mago, P.J., Chamra, L, and Steele, G. 2006. "A simulation model for the performance of a hybrid liquid desiccant system during cooling and dehumidification." International Journal of Energy Research, 30: 51-66.

Mesquita, L.C., Harrison, S., and Thomey, D. 2006. "Modeling of heat and mass transfer in parallel plate liquid-desiccant dehumidifiers." Solar Energy, 80: 1475-1482.

Park, M.S., Howell, J.R., Vliet, G.C., and Peterson, J. 1994. "Numerical and experimental results for coupled heat and mass transfer between a desiccant film and air in cross-flow." International Journal of Heat and Mass Transfer, 37 (Supp 1): 395-402.

Rahamah, A., Elsayed, M.M., and Al-Najem, N.M. 1998. "A numerical solution for cooling and dehumidification of air by a falling desiccant film in parallel flow." Renewable Energy, 13 (2): 305-322.

Ullah, M.R., Kettleborough, C.F., and Gandhidasan, P. 1967. "Studies on the lithium chloride-water absorption refrigeration machine." Technology Reports of Kansas University, No. 9: 71-84.

Wimby, M.J., and Berntsson, T.S. 1994. "Viscosity and density of aqueous solutions of LiBr, LiCl, $ZnBr_2$, $CaCl_2$, and $LiNO_3$." Journal of Chemical and Engineering Data, 39 (1): 68-74.

Zaytsev, I.D. and Aseyev, G.G. 1992. Properties of Aqueous Solutions of Electrolytes. CRC Press: Boca Raton.

APPENDIX A

MODEL IMPLEMENTATION

The model was implemented using LabVIEW software. The program was developed with a user interface that calls to a program for the specified flow arrangement. The programs for each the flow arrangement call to a program that executes the calculations outlined in section 2.1 for a control volume. Figure A.1 illustrates this hierarchy.

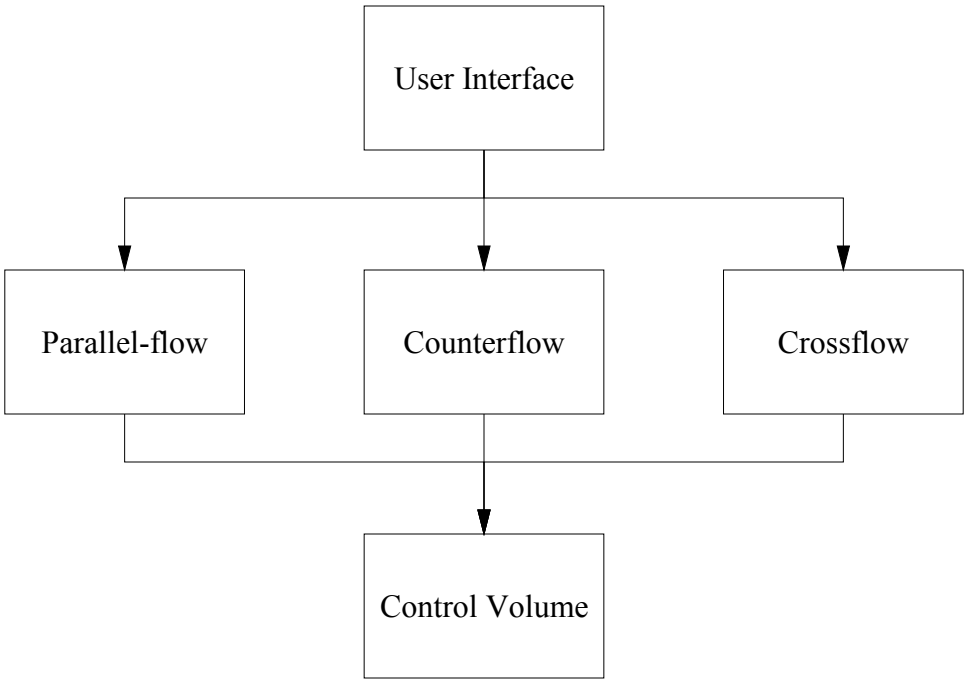

Figure A.1 Hierarchy of program

The user interface, pictured in Figure A.2, allows the user to select the desiccant type, flow arrangement, absorption process, pressure, inlet conditions for the air and desiccant solution, and uncertainty values. In addition, the user has the option to specify the Nusselt number, heat transfer coefficient, or mass transfer coefficient. From the interface the user can update the exiting conditions for the air and desiccant solution, calculate the relative uncertainty in the exiting humidity ratio, or perform a range analysis.

When updating the exiting conditions the output values for each control volume along with other calculated information, such as property values, are displayed in a different tab. For the range analysis the user selects the range parameter, the high and low values for the parameter, and the number of points. From this information the program will graph the output data. There is also an option to save the range data, control volume data, or *UMF* values.

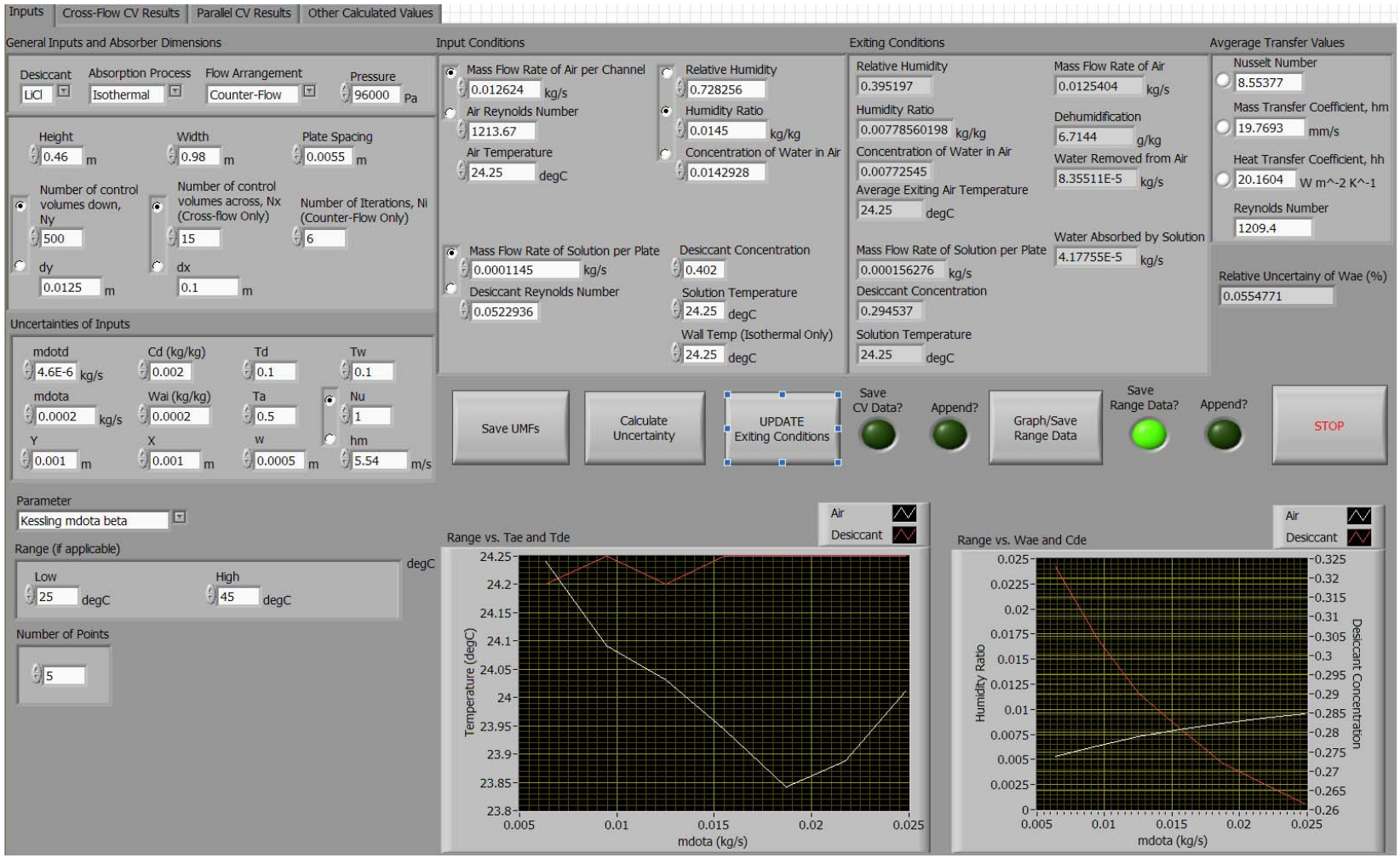

Figure A.2 LabVIEW user interface for program

APPENDIX B

PROPERTY VALUES OF DESICCANT SOLUTIONS

B.1 Property Values of LiCl

The density of LiCl, as proposed by Wimby and Berntsson (1994), is given by the expression

$$\begin{aligned} a_0 &= 1002.8 & a_1 &= -0.15582 & a_2 &= -0.00288358 \\ a_3 &= 6.1378 & a_4 &= 0.058452 & a_5 &= 0.0006065 \\ a_6 &= -0.00012546 & a_7 &= 0.000058029 & a_8 &= 0.0026623 \\ a_9 &= -0.000025941 \end{aligned}$$

$$\rho_d = \left[\begin{aligned} & a_0 + a_1 T_d + a_2 T_d^2 + a_3 C_d^{\%} + a_4 (C_d^{\%})^2 + a_5 T_d C_d^{\%} \\ & \quad + a_6 T_d (C_d^{\%})^2 + a_7 T_d^2 C_d^{\%} + a_8 (C_d^{\%})^3 + a_9 (C_d^{\%})^4 \end{aligned} \right] \frac{kg}{m^3} \tag{B.1}$$

where $C_d^{\%}$ is the concentration of the desiccant expressed as a percent. The viscosity, specific heat, and vapor pressure all follow the polynomial relation of

$$prop = (a_0 + a_1 T_d + a_2 T_d^2) + (b_0 + b_1 T_d + b_2 T_d^2) C_d + (c_0 + c_1 T_d + c_2 T_d^2) C_d^2 \tag{B.2}$$

The coefficients for the viscosity (Pa s), presented by Wimby and Berntsson (1994), are

$$\begin{aligned} a_0 &= 0.10473863 & a_1 &= -0.00433532 & a_2 &= 0.000051553 \\ b_0 &= -0.66240927 & b_1 &= 0.027224037 & b_2 &= -0.00032255 \\ c_0 &= 1.11651632 & c_1 &= -0.0442368 & c_2 &= 0.000515651 \end{aligned} \tag{B.3}$$

and the coefficients for the specific heat (kJ/kg-K), proposed by Zaytsev and Aseyev (1992), are

$$\begin{aligned} a_0 &= 3.90446 & a_1 &= 0.01743 & a_2 &= -0.0002647 \\ b_0 &= -3.57625 & b_1 &= -0.090554 & b_2 &= 0.001391 \\ c_0 &= 0.26192 & c_1 &= 0.11345 & c_2 &= -0.0017421 \end{aligned} \tag{B.4}$$

The vapor pressure pressure was taken from Fumo (2000), where a curve fit was done using data from Uemura (1967). For dehumidification the constants to Equation (B.2) are

$$
\begin{aligned}
a_0 &= 4.58208 \quad & a_1 &= -0.159174 \quad & a_2 &= 0.0072594 \\
b_0 &= -18.3816 \quad & b_1 &= 5.661 \quad & b_2 &= -0.019314 \\
c_0 &= 21.312 \quad & c_1 &= -0.666 \quad & c_2 &= 0.01332
\end{aligned}
\tag{B.5}
$$

and those for the regeneration process are

$$
\begin{aligned}
a_0 &= 16.294 \quad & a_1 &= -0.8893 \quad & a_2 &= 0.01927 \\
b_0 &= 74.3 \quad & b_1 &= -1.8035 \quad & b_2 &= -0.01875 \\
c_0 &= -226.4 \quad & c_1 &= 7.49 \quad & c_2 &= -0.039
\end{aligned}
\tag{B.6}
$$

B.2 Property Values of $CaCl_2$

Table B.1 Property values of $CaCl_2$ published in Mesquita et al. (2006)

	$CaCl_2$
k (W/m-K)	0.525
c_p (J/kg-K)	2330
ρ (kg/m^3)	1394
μ (kg/m-s)	1.19E-02
D (m^2/s)	2.50E-05

The vapor pressure of $CaCl_2$, in Pa, where the saturation pressure of water vapor is evaluated using the desiccant temperature, $P_{sat}^{T_d}$, is given by Rahamah et al. (1997) as

$$
P_{v.d} = P_{sat}^{T_d}\left(1.0 - 0.828C_d - 1.496C_d^2 + C_d\frac{T_d - 40}{350}\right) \tag{B.7}
$$